

**MODELLING OF MATERIAL PROPERTIES CRITICAL TO  
PROCESS SIMULATION**

**Z. Guo, N. Saunders, J.P. Schillé and A.P. Miodownik**

**Sente Software Ltd, Surrey Technology Centre, Guildford GU2 7YG, U.K.**

**SUMMARY**

Process simulation requires accurate and reliable data for a wide variety of material properties, ranging from thermal conductivity to flow stress curves. Traditionally such data are gathered from experimental sources, which has significant disadvantages in that not all of the required data is readily available, it may be from various sources that are themselves inconsistent, measurement of high temperature properties is expensive, and furthermore the properties can be sensitive to microstructure as well as to alloy composition. Therefore, it is highly desirable to develop computer models that can calculate all relevant material properties required by process simulation.

This paper describes the development of a computer model that can provide many of the properties required by process simulation in multi-component commercial alloys. These properties are wide ranging, including

- Thermo-physical and physical properties (from room temperature to the liquid state), such as density, thermal expansion coefficient, thermal conductivity, Young's/shear/bulk moduli, Poisson's ratio, viscosity, specific heat and enthalpy.
- Temperature and strain rate dependent mechanical properties up to the liquid state, including high temperature strength and flow stress-strain curves.
- Physical and mechanical properties of steels as a function of time, temperature and cooling rate including user-defined cooling profiles.

A key advantage of the present approach is that detailed property information can be obtained for each phase when necessary. The calculations are based on sound physical principles rather than purely statistical methods, thus many of the shortcomings of methods such as regression analysis have been avoided.

The material properties calculated by JMatPro are displayed conventionally but can also be directly exported to FE/FD based casting or forging simulation packages.

**KEYWORDS:** Modelling, material data, process simulation, TTT/CCT diagrams, high temperature properties

# MATERIALS DATA FOR PROCESS SIMULATION

## INTRODUCTION

Material data is a vital input for finite-element (FE) finite difference (FD) based process simulation. Such data include physical, thermo-physical and mechanical properties, all as a function of temperature. While these properties are relatively easy to measure at room temperature, they become increasingly difficult to determine experimentally at high temperatures. It is therefore no surprise that lack of material data has been a common problem for all FE simulation packages. To overcome this problem and provide reliable and cost effective data for process simulation, computer-based models are required so that such properties can be readily calculated. The present paper provides background to a new software package JMatPro [1,2,3,4,5] that is able to provide many of the properties required in multi-component alloys, concentrating on three areas:

- Solidification properties critical to casting simulation.
- High temperature strength and stress-strain curves.
- Phase transformations and material properties leading to the prediction of quench distortion in steels.

To make JMatPro's material data more easily used by process modellers, the data can now be organised in such a format that can be directly read by FE simulation packages. Such linking has been successfully developed between JMatPro and casting and forging simulation packages and subsequently extended to heat treatment and welding simulation packages.

### **1: Solidification Properties Critical to Casting Simulation**

Thermo-physical and physical properties of the liquid and solid phases during solidification are critical data for casting simulations. Such properties include the fraction solid, heat release, thermal expansion coefficient, thermal conductivity, density and viscosity, all as a function of temperature. However, the number of alloys for which such information is experimentally determined is limited. Within the framework of the development of JMatPro, extensive work has been carried out on the development of sound, physically based models for these properties [3,4,5]. As well as providing comprehensive data for all critical properties, it is possible to examine (a) how changes in the composition of an alloy within its specification range affect properties during solidification, and (b) how properties of the liquid vary in the mushy zone, rendering simple extrapolation of high temperature experimental data inadequate for estimating properties in the mushy zone.

The first example is the Al-alloy ADC12 (Japanese designation). This is a high Si and Cu alloy with quite large variations of the admissible levels of elements such as Cu, Fe, Ni and Si. Two compositions have been tested; one at the minimum level specified for each element, the other the maximum level.

## MATERIALS DATA FOR PROCESS SIMULATION

Figure 1 shows fraction solid vs. temperature plots calculated for the two alloys. The high specification (HS) alloy is hypereutectic, with primary Si and intermetallics forming over a significant temperature range, while the low specification (LS) alloy forms about 22% primary Al. At the start temperature of eutectic solidification for the HS alloy (565°C) the fraction solid for the LS alloy is ~65%, in comparison to ~5% for the HS alloy. The discrepancies between fraction solid at any temperature remain high for much of the solidification sequence, though both finally solidify via a eutectic involving  $\text{Al}_2\text{Cu}$ . Due to the very different behaviour of the two alloys, there will be a subsequent effect on all of the properties as a function of temperature. An example is the volume change in the range 450-650°C, which again is quite different for the two alloys (Figure 2).

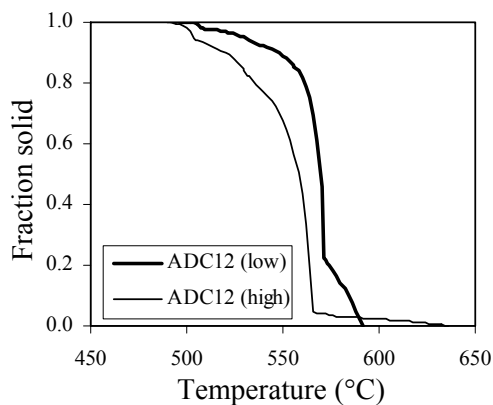


**Figure 1. Calculated fraction solid vs. temperature for two ADC12 Al-alloys**

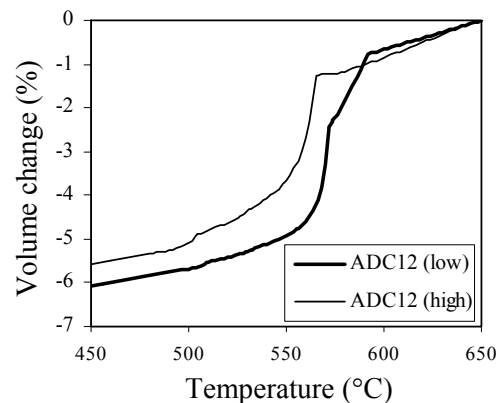


**Figure 2. Calculated volume change vs. temperature for two ADC12 Al-alloys**

Differences between alloys with much smaller composition variations can still produce quite substantial variations in the properties of the liquid within the freezing range. The Al-alloy 356 is taken as an example here. Figure 3 shows the density changes of an alloy with the composition Al-0.01Cu-0.2Fe-0.3Mg-0.02Mn-7Si-0.025Zn (wt%). For this composition, there is a slight density inversion as Mg segregates into the liquid below the silicon eutectic. However, when Cu, Mn and Zn levels increase to (0.25%Cu, 0.3Mn, 0.35Zn) the behaviour of the liquid in the mushy zone changes dramatically (Figure 4). The initial dendritic Al solidification is very similar; however the behaviour during the eutectic part of solidification is quite different, with the liquid phase now being much denser. The viscosity is also strongly affected and both effects will strongly affect liquid flow in the dendrite arms and hence defect formation.

## MATERIALS DATA FOR PROCESS SIMULATION

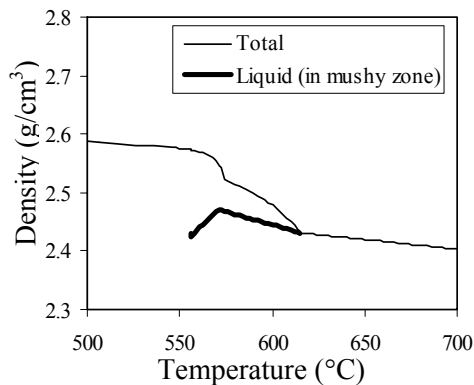


Figure 3. Calculated density of a 356 Al-alloy (with low Cu, Mn and Zn) during solidification.

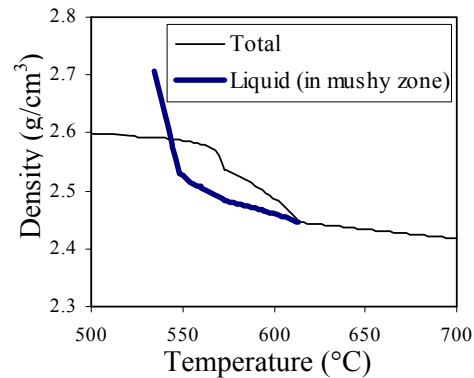


Figure 4. Calculated density of a 356 Al-alloy (with high Cu, Mn and Zn) during solidification.

While, in the case of 356, the fraction solid vs. temperature behaviour changes little, the change in the liquid properties in the mushy zone has significant impact on defect formation. This is demonstrated using the MAGMASOFT® casting simulation package where distinct differences in hotspot behaviour are predicted to occur.

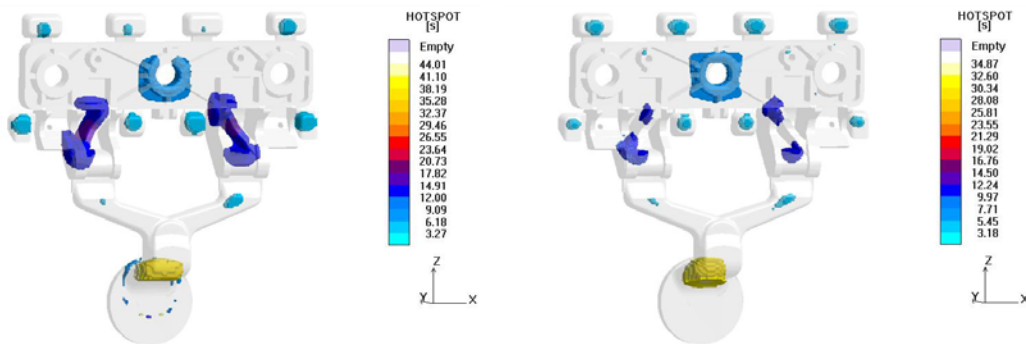


Figure 5. Comparison of calculated hotspots for casting of a 356 Al-alloy with differing levels of Cu, Mn and Zn (courtesy MAGMA GmbH)

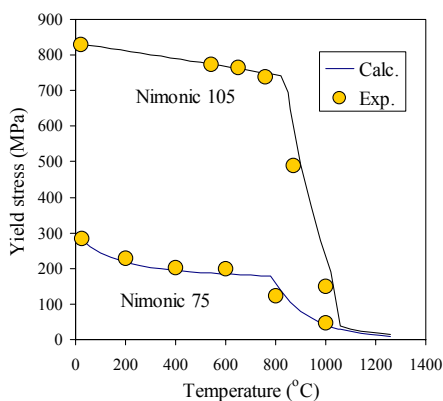
## 2: High Temperature Strength and Stress/Strain Curves

A key element in process modelling of metallic alloy is their high temperature mechanical behaviour, particularly with respect to flow stress as a function of temperature and strain rate. Many attempts at modelling flow behaviour in metals are based constitutive equations, which are fitted to experimental results. This allows some extrapolation from the regime of temperature and strain rate of the experiment, but confidence in the result when well away from the experimental regime declines considerably. It is therefore of substantial interest to develop physically based models that can be self-consistently applied and which can both account for known experimental data and be extrapolated into new and very different regimes with greater confidence.

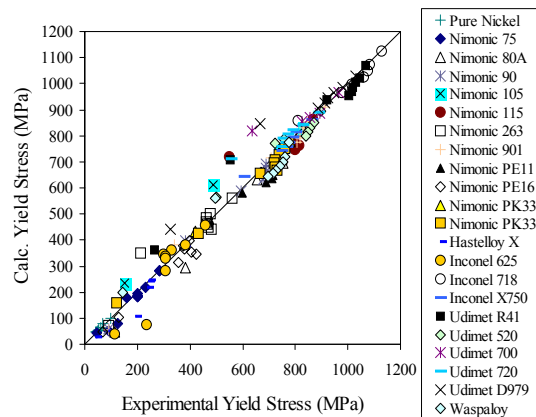
## MATERIALS DATA FOR PROCESS SIMULATION

The strength modelling in JMatPro is based on well-established equations for low temperature yield (LTY) and the classic Hall-Petch equation to provide strength as a function of grain size [1,2,5]. The model has been validated for many types of alloys, including steels, Ti- and Ni-based alloys. Precipitation hardening models have also been developed and tested for Ni-based alloys [1,2,5] and will be extended to more general cases, such as carbide hardening.

Generally speaking, room temperature strength decays monotonically with increasing temperature until the point where it enters into a temperature regime whereby there is a sharp fall in strength and flow stress becomes much more strongly dependent on strain rate. This region coincides with the stress/temperature range where flow is governed by creep [1,2,5]. Several relationships between visco-plastic flow and creep are available in the literature [6,7], but the perceived difficulty in obtaining the necessary input parameters to creep equations means that this research area has not been well developed. JMatPro has developed creep models based on classic formulations that have been extensively validated against experiment for steels and Ni-based superalloys. Also, because the input parameters are physically based (e.g. diffusion mechanisms, fault energies), they provide a much greater ability to be used outside of previously measured stress/strain rate/temperature regimes.



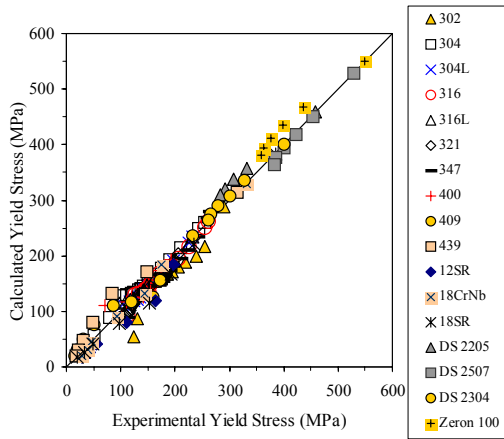
**Figure 6. Comparison between experimental and calculated yield stress for Nimonic 75 and 105 as a function of temperature.**



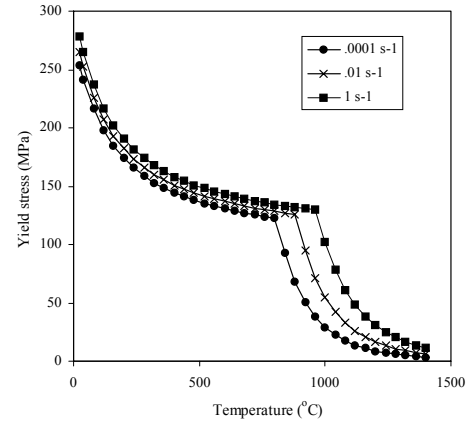
**Figure 7. Comparison between experimental and calculated yield stress of wrought superalloys and pure Ni from RT to 1000°C**

Figure 6 shows the yield stress of two Ni-based superalloys, one precipitation hardened by  $\gamma'$  (Nimonic 105), the other a solid solution alloy (Nimonic 75). The model correctly predicts the transition where sudden softening occurs and also accounts for the loss of strength as the  $\gamma'$  dissolves and the alloy eventually becomes a solid solution. Figure 7 shows the calculated yield stress against experiments between room temperature (RT) and 1000°C for 22 commercial superalloys, ranging from pure nickel, highly alloyed solid solution types such as the Hastelloy series to high  $\gamma'$  type alloys such as the Udimet series that can contain up to 50%  $\gamma'$ .

## MATERIALS DATA FOR PROCESS SIMULATION



**Figure 8. Comparison between experimental and calculated yield stress for various stainless steels between RT and 900°C.**



**Figure 9. Calculated yield stresses for a 316 stainless steel as a function of strain rate and temperature.**

Figure 8 is a comparison plot of calculation vs. experiment for stainless steels, including austenitic, ferritic and duplex types. Flow stress as a function of strain rate has also been calculated and Figure 9 shows such a series of calculated yield stress for a 316 stainless steel as the strain rate is increased from  $0.0001 \text{ s}^{-1}$  to  $1 \text{ s}^{-1}$ . The transition from a dislocation yield mechanism to a creep controlled mechanism is clearly observed and is substantially displaced. However, even at a rate of  $1 \text{ s}^{-1}$ , creep is still the dominant mechanism above  $1000^\circ\text{C}$ . Of particular interest is to note that the strain rate dependency at any temperature in the creep controlled regime is substantially greater than in the dislocation yield controlled regime. For example at  $1100^\circ\text{C}$ , the yield stress increases by almost a factor 4 between  $0.0001$  and  $1 \text{ s}^{-1}$ .

The secondary creep model, which has been described previously [8], has been extended to include primary and tertiary creep. It is now therefore possible to calculate full creep curves as a function of applied stress, which then allows the construction of a 3-dimensional surface that has as its axes stress, strain and time. Assuming that the strain-rate in a tensile test and the creep rate in creep testing are interchangeable, it is then possible to calculate stress/strain curves at specific strain rates. Combining this procedure with stress/strain curves calculated for the LTY region [9] allows stress/strain curves to be calculated over the full range of temperatures, potentially including the mushy zone.

The extended creep model used here follows the work of [10] which describes primary creep as:

$$\dot{\epsilon}_p = \frac{\dot{\epsilon}_s}{K} \ln \left[ 1 + \frac{\dot{\epsilon}_i - \dot{\epsilon}_s}{\dot{\epsilon}_s} (1 - e^{-Kt}) \right] \quad (1)$$

## MATERIALS DATA FOR PROCESS SIMULATION

Where  $\dot{\epsilon}_p$  and  $\dot{\epsilon}_s$  are respectively the primary and secondary creep rates,  $\dot{\epsilon}_i$  is the initial creep rate and  $K$  is an empirically evaluated materials constant. In the present case we have made  $\dot{\epsilon}_i = b\dot{\epsilon}_s$ , where  $b$  is a simple proportionality constant. To account for tertiary creep we have used a somewhat empirical model that relates the tertiary creep rate to the secondary rate and the creep rupture life.

$$\dot{\epsilon}_t = \dot{\epsilon}_s t \left[ 2C_d (t/R_l)^4 \right] \quad (2)$$

where  $\dot{\epsilon}_t$  is the tertiary creep rate,  $C_d$  is a "damage constant" and  $R_l$  is the rupture life, which can be readily calculated by combining the secondary creep rate and a Monkman-Grant type relationship [8].

The behaviour of a 718 Ni-based superalloy in the high temperature  $\gamma$  phase field is used to demonstrate our approach, where these alloys are thermo-mechanically processed. Figure 10 show comparison of calculated and experimentally observed flow stresses [11,12,13,14] at various strains over a wide range of temperatures for 718.

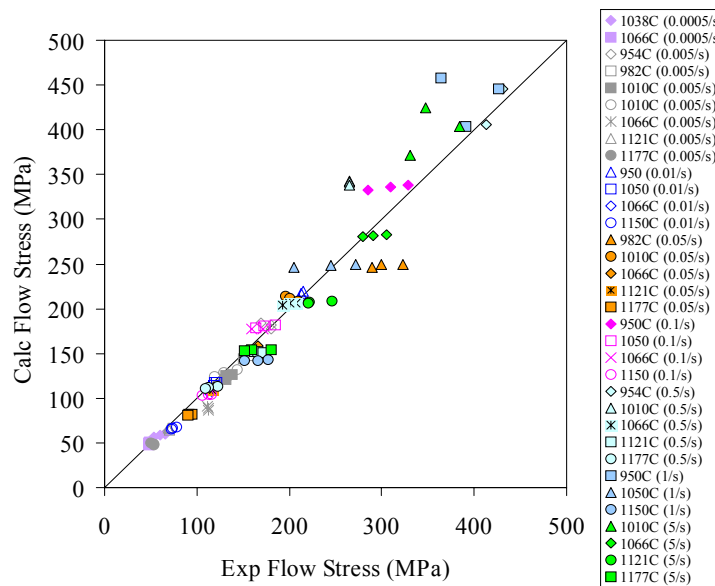


**Figure 10. Comparison plot of calculated vs. experimental flow stress [11,12,13,14,] at various strain rates and temperatures for 718.**

### 3: Phase Transformations and Material Properties Leading to the Prediction of Quench Distortion in Steels

Distortion induced by heat treatment is a major industrial problem because it critically affects the dimensional accuracy of precision components. Prediction of distortion is difficult because it requires detailed knowledge of the material properties which are normally lacking and difficult to evaluate, especially at high temperatures. This part of the paper describes the model development for prediction of the material properties required for distortion prediction in steels. The success of the model is based on accurate description of all the major phase transformations taking place, as well as an accurate calculation of the properties of different phases formed during heat treatment. The model calculates a wide range of physical, thermo-physical and mechanical properties, all as a function of time/temperature/cooling rate.

Significant work has been undertaken over recent decades to develop models that can calculate TTT and CCT diagrams for steels [15]. However, almost without exception, these models have been shown to be limited in applicability to carbon and low alloy steels. One of the advantages of the present model is that it can provide accurate TTT and CCT diagrams for a much wider range of steels, including medium to high alloy types, tool steels and 13%Cr steels. By linking such calculations to JMatPro's property models a complete set of physical and mechanical properties can be calculated for steels as a function of time/temperature/cooling rate, including user-defined cooling profiles.

It should be noted that the amounts of martensite and bainite are affected by changes in composition of the parent austenite, which may result from prior ferrite formation or carbide precipitation at the austenisation temperature. This has been considered in the present calculation of phase evolution. Examples given below demonstrate how cooling rate affects the physical and thermo-physical properties of a steel 4140 with grain size ASTM 7~8). Figure 11 shows the evolution of various phases during cooling at 20 °C/s and 1 °C/s, respectively. The influence of cooling rate on phase transformations is clearly demonstrated.

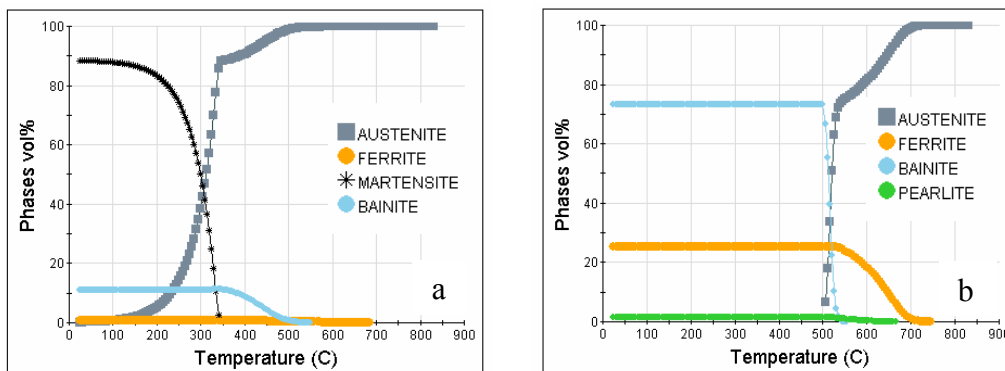


**Figure 11. Microstructure evolution in 4140 during cooling at (a) 20°C/s and (b) 1°C/s**

## MATERIALS DATA FOR PROCESS SIMULATION

It is quite simple to transform the model such that it calculates phase formation as a function of time and temperature during a cooling cycle. The cooling path can be quite arbitrary, including isothermal hold times at constant temperature, if required. For demonstration purposes we have chosen a 4140 US grade steel and calculated various properties on heating and at cooling rates ranging from 0.01 to 100  $\text{K s}^{-1}$ , Figure 12.

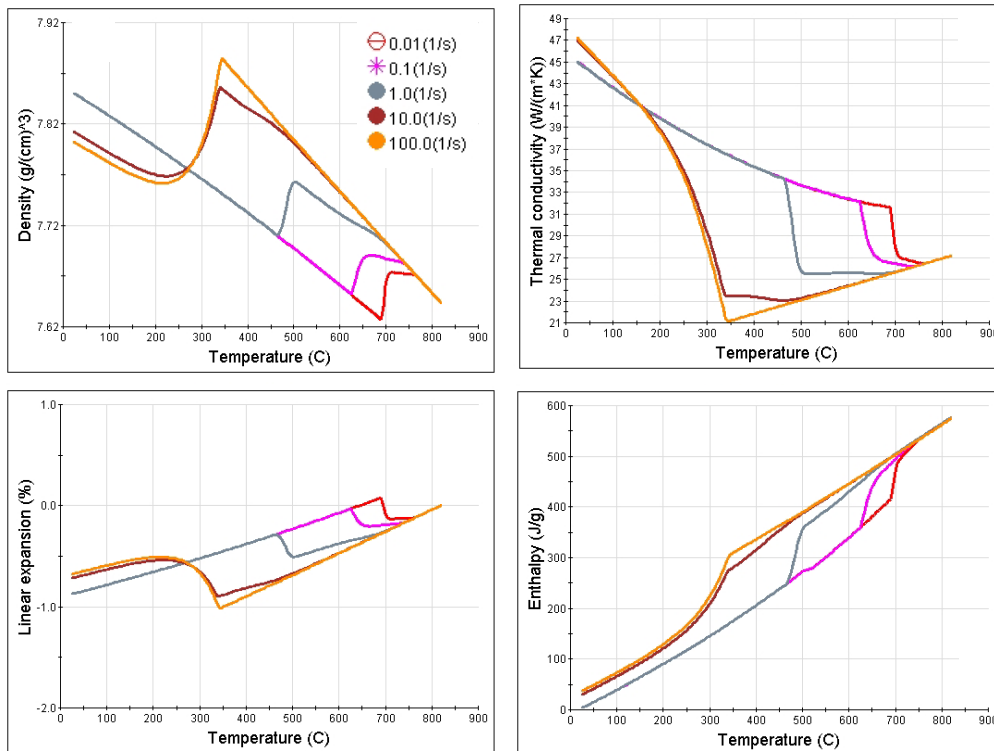


**Figure 12. Various properties calculated for a 4140 steel at various cooling rates ranging from 0.01 to 100 °C/s.**

The mechanical properties of steels during cooling can be calculated as a function of cooling rate and temperature. The hardness and strength of various phases such as ferrite, austenite, pearlite, bainite and martensite have been calculated [16,17] first and then they are used to calculate the overall strength and hardness of the alloy. Using steel 4140 as an example, the influence of cooling rate on yield strength is shown in Figure 13. The yield strength at 100 and 10 °C/s are very close due to the fact that the majority phase is martensite in both cases. It should be mentioned that by clicking a strength point in the curve, the stress-strain curve for that position will be generated. The strength vs. temperature of each phase can be provided as well.

## MATERIALS DATA FOR PROCESS SIMULATION

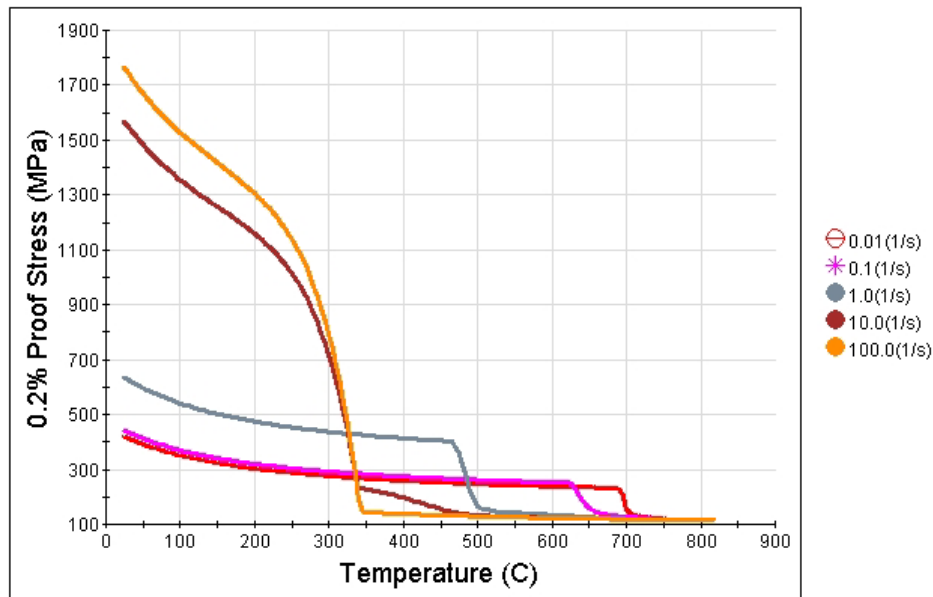


Figure 13. Yield stress for a 4140 steel at various cooling rates ranging from 0.01 to 100 °C/s.

### 4: Linking JMatPro with FE-based Simulation Packages

Material data calculated by JMatPro have been used by users of many FE/FD-based simulation packages, e.g. MAGMASOFT® or ProCast® for casting, DEFORM® and Forge-3D® for forging and rolling, and ANSYS® as a general tool. To make JMatPro's data more easily used by process modellers, new subroutines have been created within JMatPro so that the property data will be written as files that can be directly used by the simulation packages. Such linking has been successfully developed between JMatPro and the software packages mentioned previously and is being subsequently extended to heat treatment and welding simulation packages.

### 5: Summary

The paper has shown how a new software programme, JMatPro, has been able to calculate a variety of material properties and behaviour for multi-component alloys. In particular, the paper has concentrated on JMatPro's capability for solidification properties for casting simulation, high temperature mechanical properties for forging/rolling simulation, and phase transformations and material properties leading to the prediction of quench distortion in steels. Links between JMatPro and many FE-based process simulation packages have been established successfully and JMatPro's property data can now be organised in such a format that can be directly read by those packages.

## MATERIALS DATA FOR PROCESS SIMULATION

### REFERENCES

---

- [1] SAUNDERS N, LI X, MIODOWNIK A P and SCHILLE J P, Materials Design Approaches and Experiences, Eds. ZHAO J C et al., TMS, Warrendale, PA, 2001, p. 185
- [2] SAUNDERS N, GUO Z, LI X, MIODOWNIK A P and SCHILLE J P, JOM, Vol 55, No 12, 2003, p. 60
- [3] SAUNDERS N, LI X, MIODOWNIK A P and SCHILLE J P, Modelling of Casting, Welding and Advanced Solidification Processes X, Eds Stefanescu D et al., TMS, Warrendale, PA, 2003, p. 669
- [4] GUO Z, SAUNDERS N, MIODOWNIK A P and SCHILLE J P, Modelling of Casting and Solidification Processes 2004, Ed Hwang W S, Metal Industrials Research and Development Centre, Kaohsiung, Taiwan, 2004, p. 563
- [5] SAUNDERS N, GUO Z, LI X, MIODOWNIK A P and SCHILLE J P, Superalloys 2004, Eds Green K A et al., TMS, Warrendale, PA, 2004, p. 849
- [6] HARSTE K and SCHWEDTFEGER K, Mater. Sci. Tech., Vol 8, 1992, p. 23
- [7] HARSTE K and SCHWEDTFEGER K, Mater. Sci. Tech., Vol 12, 1996, p. 378
- [8] MIODOWNIK A P, LI X, SAUNDERS N and SCHILLE J P, Parsons 2003: Engineering Issues in Turbine Machinery, Power Plant and Renewables, Eds Strang A et al., London: Inst.MMM, 2003, P. 779
- [9] LI X, MIODOWNIK A P and SAUNDERS N, J. Phase Equilibria, Vol 22, 2001, p. 247
- [10] LI J C M, Acta Metall., Vol 11, 1963, p. 1269
- [11] WEIS M J, MATAYA M C, THOMPSON S W and MATLOCK D K, Superalloy 718, Ed Loria E A, Warrendale, PA: TMS, 1989, p. 135
- [12] GARCIA C I, WANG G D, CAMUS D E, LORIA E A and DEARDO A J, Superalloys 718,625, 706 and Various Derivatives, Ed Loria E A, Warrendale, PA: TMS, 1994, p. 293
- [13] ZHAO D, GUILLARD S and MALE A T, Superalloys 718,625, 706 and Various Derivatives, Ed Loria E A, Warrendale, PA: TMS, 1997, p. 193
- [14] PARK N K, YUM J T, NA Y S, KIM I S, KIM D H and CHOE S J, Superalloys 718,625, 706 and Various Derivatives, Ed Loria E A, Warrendale, PA: TMS, 1997, p. 173
- [15] KIRKALDY J S and VENUGOPOLAN D, Phase Transformations in Ferrous Alloys, Eds Marder A R and Goldstein J I, AIME, Warrendale, PA, 1984, p. 125
- [16] GUO Z, SAUNDERS N, MIODOWNIK A P and SCHILLE J P, 2<sup>nd</sup> International Conference on Heat Treatment and Surface Engineering in Automotive Applications, 20-22 June, 2005, Riva del Garda, Italy
- [17] LI X, MIODOWNIK A P, SAUNDERS N, Mater. Sci. Technol., Vol 18, 2002, p. 861